Photothermal Infrared Imaging: Identification and Visualization of Micro- and Nanoplastics in Environmental Matrices

Ilia M. Pavlovetc^{a,†,*}, Kirill Kniazev^{a,†}, Junyeol Kim^b, Kyle Doudrick^{b,*}, and Masaru Kuno^{a,c,*}

 $^{\rm a}{\rm Department}$ of Chemistry and Biochemistry, University of Notre Dame, Notre Dame, IN $46556{\rm ,USA}$

^bDepartment of Civil and Environmental Engineering and Earth Sciences, University of Notre Dame, Notre Dame, IN 46556

^cDepartment of Physics, University of Notre Dame, Notre Dame, IN 46556, USA

ABSTRACT

Infrared photothermal heterodyne imaging (IR-PHI) is an established all-optical, table-top approach for conducting super-resolution mid-infrared microscopy and spectroscopy on submicrometer-sized particles. The instrument's capabilities are highlighted by its ability to operate in spectroscopically-crowded environments. This includes specimens obtained from environmental matrices where particulates with different morphologies, chemical compositions, and abundances exist. Here, proof-of-concept IR-PHI measurements have been conducted on anthropogenic micro- and nanoplastics (MNPs) derived from the breakdown of consumer products. In particular, IR-PHI is used to characterize MNPs extracted from steeped plastic teabags and floor dust from a household vacuum. IR-PHI results reveal the presence of complex MNP structures made of polyamide fibers and acrylonitrile butadiene styrene MNPs.

Keywords: Photothermal imaging, Infrared spectroscopy, Microplastics, Infrared Microscopy, Super-resolution imaging, Nanoplastics

1. INTRODUCTION

Plastics are ubiquitous in modern society. Inevitable degradation results in the presence of micro- and nanoplastics (MNPs) in the world's seas, oceans, mountains, and urban environments. Recent reports additionally reveal the intended and unintended presence of MNPs in consumer products, including tea, infant feeding bottles, seafood, between the salt, beverages, cosmetics, and toothpaste. There is growing concern, about the effects of MNPs on human health, separately given their small size (0.01-100 μ m) and chemical complexity.

MNPs have been studied using various analytical techniques. No single approach, however, fully accounts for their complexity in terms of size, morphology, chemical composition, and environmental fate. Thermal analyses provide data on polymer type and information regarding the presence of chemical additives. They are destructive, though, and require complex data deconvolution due to overlapping thermal transitions. ^{17–19} Thermal decomposition techniques additionally yield only total mass data for MNPs. MNP sizing and counting lie beyond its capabilities. In contrast, electron microscopies readily characterize NMP size and shape. However,

I.M.P.: E-mail: ipavlove@nd.edu K.D.: E-mail: kdoudrick@nd.edu M.K.: E-mail: mkuno@nd.edu

[†]I.M.P. and K.K. contributed equally;

^{*}Further author information: (Send correspondence to I.M.P., K.D., or M.K.)

they provide highly restrictive chemical information. This results in a high percentage of false positives when trying to identify MNPs.¹⁹

Vibrational spectroscopies/microscopies such as Fourier Transform Infrared (FTIR) or Raman are non destructive techniques, and more relevantly, provide chemical specificity. Unfortunately, their spatial resolution is limited by the optical diffraction limit to values on the order of half the wavelength of light. For FTIR, this means length scales on the order of $\sim 5~\mu m$. For Raman, use of a visible laser results in an improved spatial resolution of order $\sim 300~nm$. Raman, however, is less sensitive than infrared (IR) absorption given small scattering cross-sections $\sim 10~orders$ of magnitude smaller than corresponding infrared absorption cross-sections. Raman additionally suffers from interference due to specimen autofluorescence.

We have recently developed a far-field, super-resolution IR imaging technique, called IR Photothermal Heterodyne Imaging (IR-PHI). The technique is capable of chemically characterizing individual particles. $^{20-30}$ Of note is that IR-PHI possesses a spatial resolution below the IR diffraction limit. $^{23,28,31-34}$ Its operating principle is the detection of photothermal changes induced in a specimen following its absorption of IR radiation. IR-PHI's super-resolution (~ 300 nm) comes from its use of a visible "probe" laser to quantify induced photothermal changes. IR-PHI is also notable in that it reports on specimen IR absorption as opposed to extinction. This is important in microparticle studies to avoid unwanted Mie scattering artifacts. 35,36 Olson *et al.* have exploited this to perform physicochemical and spectroscopic analyses of ambient aerosol particles over a vast range of sizes $(0.4-5~\mu\text{m})$. 37

Here, we apply IR-PHI to identify and characterize MNPs in environmental matrices. The study comprises of two samples with varying degrees of complexity. The first involves MNPs, leached from plastic teabags.³ The second demonstrates IR-PHI's analytical possibilities by testing its imaging and spectroscopic capabilities on untreated household vacuum dust. Both are thought to contain MNPs, linked to the degradation of plastic-containing consumer products such as nylon teabags, plasticware, and carpet.

2. MATERIALS AND METHODS

IR-PHI measurements. The IR-PHI setup consists of a tunable, pump laser, which is a pulsed ($\lambda = 5.4 - 9.6 \mu m$, $\tilde{\nu} = 1040 - 1840 \text{ cm}^{-1}$) mid-infrared optical parametric oscillator (OPO, M Squared Lasers). A continuous wave (CW), 532 nm, diode-pumped solid state laser serves as the probe. The OPO output is focused onto a specimen coverslip using a reflective objective (Ealing, 0.65 NA). Probe light is focused onto the same spatial location using a refractive objective (Nikon, 0.95 NA). Objectives are arranged in a counterpropagating geometry to maximize IR-PHI's spatial resolution.²³

Samples are deposited onto CaF₂ coverslips (Crystran) and are raster scanned through mutual pump and probe focii using a closed-loop, nano-positioning stage (Mad City Labs). Scan ranges are limited to $300 \times 300 \ \mu$ m² with typical step sizes between 0.05 and 1 μ m. Corresponding pixel dwell times range from 10 to 100 ms.

Pump-induced changes to specimen refractive indices/scattering cross sections are detected via intensity modulation imprinted onto scattered probe light.²⁸ Scattered probe light is collected with the same refractive objective used to focus it and is directed onto a Si photodiode. An IR-PHI signal is then extracted using a lock-in amplifier (Zurich Instruments, MFLI) referenced to the OPO repetition rate. A detailed description of the IR-PHI instrument and operating principle can be found in Reference ²⁹.

Sample preparation. MNPs from plastic teabags were prepared using a procedure near identical that used previously.³ Locally purchased plastic teabags were cut open, emptied, rinsed with ultra pure water (UPW, 18.2 M Ω cm), and dried in a fume hood. Emptied and cleaned teabags were then steeped in boiled UPW water, cooled to 95 °C, for 5 minutes.

Floor dust was collected from a household vacuum cleaner. Samples were dispersed in UPW at an estimated concentration of $5.6~\rm g/L$ and stirred at $300~\rm rpm$ with a magnetic stirrer for $96~\rm hours$. This ensured that sample fibers/particulates were disentangled.

Specimens for IR-PHI measurements were prepared by drop casting teabag/floor dust suspensions onto ${\rm CaF_2}$ coverslips. Teabag (floor dust) suspension volumes of 1.0 mL (250 $\mu{\rm L}$) were used. ${\rm CaF_2}$ coverslips were pre-cleaned with methanol/acetone and were flamed/plasma cleaned prior to use. Before conducting imaging studies, IR-PHI spectra were first acquired on individual particles located visually on substrates. This enabled their chemical confirmation and also allowed for proper selection of IR-PHI imaging energies.

3. RESULTS AND DISCUSSION

3.1 Plastic teabags

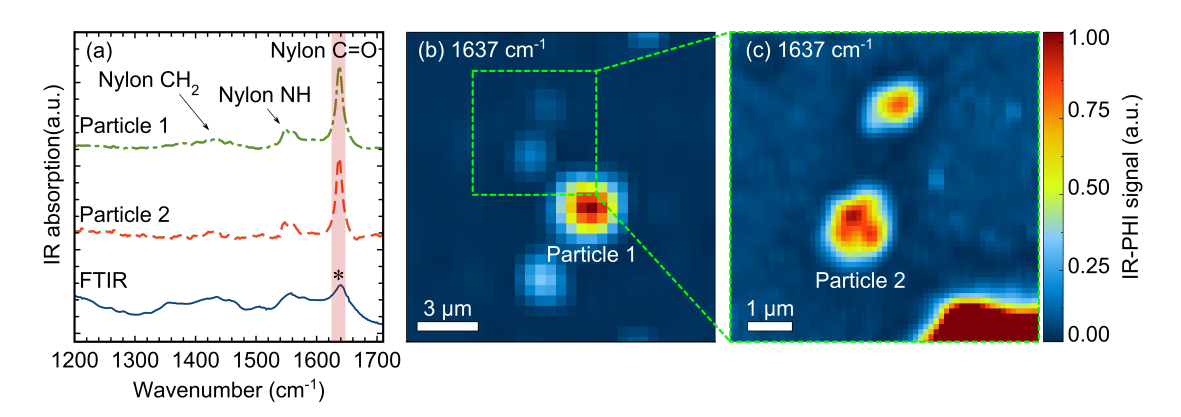


Figure 1: (a) FTIR spectrum of bulk nylon. IR-PHI spectra of individual MNP particles labeled particle 1 and particle 2. IR-PHI imaging wavenumber indicated by an asterisk. (b) Low magnification 1637 cm⁻¹ IR-PHI image of individual MNPs from a steeped 95 °C teabag suspension. (c) High magnification IR-PHI image of the marked area in panel (b).

Figure 1a first shows the FTIR spectrum of bulk nylon. Its 1637 cm⁻¹ C=O stretch has been selected for subsequent IR-PHI imaging due to its prominence. Figures 1b,c show resulting 1637 cm⁻¹ IR-PHI images of MNPs leached from 95 °C steeped plastic teabags. Specifically, Figure 1b shows a low magnification $15 \times 15 \, \mu \text{m}^2$ IR-PHI image, acquired with a step size of 500 nm and a corresponding pixel dwell time of 30 ms. The total image acquisition time is under 1 minute.

Figure 1c shows a zoomed-in $6 \times 6 \ \mu\text{m}^2$ view of the selected area in Figure 1b. A corresponding step size (dwell time) is 100 nm (100 ms) with a total acquisition time under 7 minutes. Immediately apparent are irregularly-shaped particles with the particle numbered 2 exhibiting heterogeneity in its absorption intensity. Low and high absorption regions are evident and likely stem from the particle's irregular morphology. Associated single particle IR-PHI spectra in Figure 1a reveal that all observed particles are nylon. Identical results from other areas of the same specimen confirm MNP extraction from steeped plastic teabags.

An approximate concentration of leached MNPs is 5.3×10^7 cm⁻³ from a single teabag. This value is ~ 30 times smaller than that previously reported by Hernandez et al.³ (1.5×10⁹ cm⁻³ from a single teabag). The discrepancy originates from the visualization method used to estimate leached MNP concentrations. Hernandez et al. use scanning electron microscopy (SEM) to estimate particle densities. By indirect correlation to FTIR results, they suggest that the densities obtained are leached MNP densities. Given that SEM provides no direct chemical information about the particles being observed, SEM-derived densities should be considered an upper limit. IR-PHI derived densities, by contrast, represent a lower limit since even though IR-PHI possesses chemical sensitivity and selectivity, its current detection limit restricts it to visualizing MNPs with dimensions larger than ~ 300 nm.

3.2 Floor dust

Next, despite the ubiquity of plastics in household items such as clothing and carpet as well as washing clothes being a known anthropogenic contributor to plastic waste, ^{38, 39} we know of no study that has probed for MNPs in a household environment. We have therefore examined vacuumed, household floor dust using IR-PHI to establish its applicability to studying MNPs in complex and possibly spectrally-congested environments.

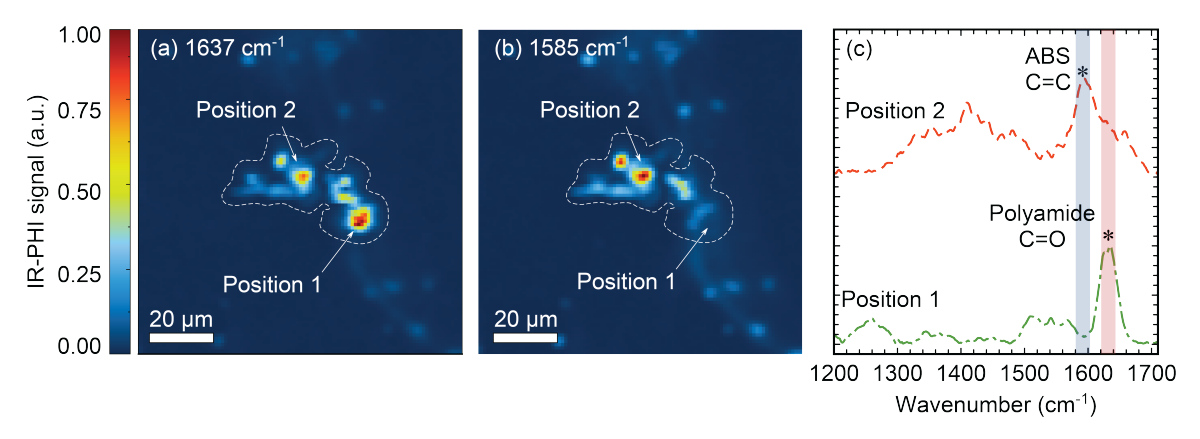


Figure 2: Same area IR-PHI images of household floor dust acquired at (a) 1637 cm⁻¹ and (b) 1585 cm⁻¹. (c) Local IR-PHI spectra of indicated regions, showing fingerprint features of both polyamide and ABS plastics. Imaging wavenumbers indicated by asterisks.

Figures 2a,b display large area $(100\times100~\mu\text{m}^2)$ IR-PHI images of floor dust imaged at 1637 cm⁻¹ and 1585 cm⁻¹. The former energy has been chosen because it corresponds to polyamide's (i.e. nylon's) prominent C=O stretching. The latter 1585 cm⁻¹ energy corresponds to a characteristic C=C aromatic ring stretching of Acrylonitrile Butadiene Styrene (ABS), a common household plastic. Images have been acquired with a step size of 1 μ m and a corresponding pixel dwell time of 30 ms. Image acquisition times are \sim 5 minutes each. The appearance of features in Figures 2a,b suggests that large and small MNP agglomerates exist in household floor dust.

To highlight IR-PHI's ability to operate in spectroscopically crowded environments, the central MNP agglomerate (highlighted by dashed white lines) is more carefully examined. Comparing **Figure 2a** to **Figure 2b** reveals that local spectral differences exist. Features imaged at 1637 cm⁻¹ are absent when imaged at 1585 cm⁻¹ and vice versa. In particular, **Figure 2a** exhibits a very strong 1637 cm⁻¹ IR-PHI signal at position 1, which disappears when imaged at 1585 cm⁻¹ (**Figure 2b**).

Local IR-PHI spectra confirm these differences. **Figure 2c** shows an IR-PHI spectrum taken at position 1. The spectrum possesses infrared transitions characteristic of ABS. Most prominent is a strong 1585 cm⁻¹ resonance, assigned to ABS's C=C aromatic ring stretch (highlighted blue). Between 1300-1500 cm⁻¹ other characteristic ABS C-C aromatic ring stretching and CH₂ bending resonances exist. This should be contrasted to a second IR-PHI spectrum, acquired at position 2. The latter spectrum shows a qualitatively different profile, which more closely resembles that of polyamide (see **Figure 1**). Of note is polyamide's characteristic 1637 cm⁻¹ C=O resonance highlighted red. Existence of both plastics in floor dust is expected as many carpets contain nylon. ABS is ubiquitous in consumer plastics.

CONCLUSIONS

We have demonstrated IR-PHI's ability to image and spectroscopically identify MNPs in two environmental matrices: steeped plastic teabag suspensions and household floor dust. The approach addresses existing analytical limitations for characterizing MNPs. Specifically, IR-PHI possesses a spatial resolution below the infrared

diffraction limit. As such, it can operate in spectroscopically congested, real world environments. IR-PHI is also sensitive and can spectroscopically interrogate individual MNP particles. Its chemical specificity further permits studies of chemical changes incurred upon MNP degradation. Future developments to IR-PHI will increase its sensitivity and along with the introduction of widefield modalities will dramatically increase its ability to identify, quantify, and study environmental MNPs.

ACKNOWLEDGMENTS

I.M.P. and M.K. acknowledge the National Science Foundation (Grant numbers CHE-1563528 and CHE-1954724) for financial support. The IR OPO system was purchased through DURIP Award W911NF1410604.

REFERENCES

- [1] Hale, R. C., Seeley, M. E., Guardia, M. J. L., Mai, L., and Zeng, E. Y., "A global perspective on microplastics," J. Geophys. Res. Oceans. 125, e2018JC014719 (2020).
- [2] Triebskorn, R., Braunbeck, T., Grummt, T., Hanslik, L., Huppertsberg, S., Jekel, M., Knepper, T. P., Krais, S., Müller, Y. K., Pittroff, M., Schmieg, A. S. R. H., Schür, C., Strobel, C., Wagner, M., Zumbülte, N., and Köhler, H. R., "Relevance of nano- and microplastics for freshwater ecosystems: A critical review," <u>TrAC-Trend Anal. Chem.</u> 110, 375–392 (2019).
- [3] Hernandez, L. M., Xu, E. G., Larsson, H. C. E., Tahara, R., Maisuria, V. B., and Tufenkji, N., "Plastic teabags release billions of microparticles and nanoparticles into tea," <u>Environ. Sci. Technol.</u> **53**, 12300–12310 (2019).
- [4] Li, D., Shi, Y., Yang, L., Xiao, L., Kehoe, D. K., Gun'ko, Y. K., Boland, J. J., and Wang, J. J., "Microplastic release from the degradation of polypropylene feeding bottles during infant formula preparation," <u>Nature</u> Food 1, 746–754 (2020).
- [5] Cauwenberghe, L. V. and R.Janssen, C., "Microplastics in bivalves cultured for human consumption," Environ. Pollut. **193**, 65–70 (2014).
- [6] Li, J., Yang, D., Jabeen, L. L. K., and Shi, H., "Microplastics in commercial bivalves from china," Environ. Pollut **207**, 190–195 (2015).
- [7] N.Bråte, I. L., P.Eidsvoll, D., Steindal, C. C., and V.Thomas, K., "Plastic ingestion by atlantic cod (gadus morhua) from the norwegian coast," Mar. Pollut. Bull. 112, 105–110 (2016).
- [8] Yang, D., Shi, H., Li, L., Li, J., Jabeen, K., and Kolandhasamy, P., "Microplastic pollution in table salts from china," Environ. Sci. Technol. 49, 13622–13627 (2015).
- [9] Liebezeit, G. and Liebezeit, E., "Synthetic particles as contaminants in german beers," <u>Food Addit. Contam.</u>
 A 31, 1574–1578 (2014).
- [10] R.Gregory, M., "Plastic 'scrubbers' in hand cleansers: a further (and minor) source for marine pollution identified," Mar. Pollut. Bull. **32**, 867–871 (1996).
- [11] Fendall, L. S. and Sewell, M. A., "Contributing to marine pollution by washing your face: Microplastics in facial cleansers," Mar. Pollut. Bull. **58**, 1225–1228 (2009).
- [12] Napper, I. E., Bakir, A., J.Rowland, S., and C.Thompson, R., "Characterisation, quantity and sorptive properties of microplastics extracted from cosmetics," Mar. Pollut. Bull. 99, 178–185 (2015).
- [13] Wright, S. L. and Kelly, F. J., "Plastic and human health: A micro issue?," Environ. Sci. Technol. 51, 6634–6647 (2017).
- [14] de S. Machado, A. A., Kloas, W., Zarfl, C., Hempel, S., and Rillig, M. C., "Microplastics as an emerging threat to terrestrial ecosystems," Glob. Chang. Biol. 24, 1405–1416 (2017).
- [15] Prata, J. C., "Airborne microplastics: Consequences to human health?," Glob. Chang. Biol. 234, 115–126 (2018).

- [16] Ragusa, A., Svelato, A., C.Santacroce, Catalano, P., Notarstefano, V., Carnevali, O., Papa, F., Rongioletti, M. C. A., Baiocco, F., D'Amore, S. D. E., Rinaldo, D., Matta, M., and Giorgini, E., "Plasticenta: First evidence of microplastics in human placenta," Environ. Int. 146, 106274 (2021).
- [17] Shim, W. J., Hong, S. H., and Eo, S. E., "Identification methods in microplastic analysis: a review," <u>Anal.</u> Methods **9**, 1384–1391 (2017).
- [18] Zarfl, C., "Promising techniques and open challenges for microplastic identification and quantification in environmental matrices," Anal. Bioanal. Chem. **511**, 3743–3756 (2019).
- [19] Elkhatib, D. and Oyanedel-Craver, V., "A critical review of extraction and identification methods of microplastics in wastewater and drinking water," Environ. Sci. Technol. **54**, 7037–7049 (2020).
- [20] Lee, E. S. and Lee, J. Y., "Nonlinear optical infrared microscopy with chemical specificity," <u>Appl. Phys.</u> Lett. 94, 261101 (2009).
- [21] Mërtiri, A., Jeys, T., Liberman, V., Hong, M. K., Mertz, J., Altug, H., and Erramilli, S., "Mid-infrared photothermal heterodyne spectroscopy in a liquid crystal using a quantum cascade laser," <u>Appl. Phys.</u> Lett. 101, 044101 (2012).
- [22] Totachawattana, A., Liu, H., Mertiri, A., Hong, M. K., Erramilli, S., and Sander, M. Y., "Vibrational mid-infrared photothermal spectroscopy using a fiber laser probe: asymptotic limit in signal-to-baseline contrast," Opt. Lett. 41, 179–182 (2016).
- [23] Li, Z., Aleshire, K., Kuno, M., and Hartland, G. V., "Super-resolution far-field infrared imaging by photothermal heterodyne imaging," J. Phys. Chem. B 121, 8838–8846 (2017).
- [24] Chatterjee, R., Pavlovetc, I. M., Aleshire, K., and Kuno, M., "Single semiconductor nanostructure extinction spectroscopy," J. Phys. Chem. C 129, 16443–16463 (2018).
- [25] Chatterjee, R., Pavlovetc, I. M., Aleshire, K., Hartland, G. V., and Kuno, M., "Subdiffraction infrared imaging of mixed cation perovskites: Probing local cation heterogeneities," <u>ACS Energy Lett.</u> 3, 469–475 (2018).
- [26] Pavlovetc, I. M., Brennan, M. C., Draguta, S., Ruth, A., Moot, T., Christians, J. A., Aleshire, K., Harvey, S. P., Toso, S., Nanayakkara, S. U., Messinger, J., Luther, J. M., and Kuno, M., "Suppressing cation migration in triple-cation lead halide perovskites," ACS Energy Lett. 5, 2802–2810 (2020).
- [27] Aleshire, K., Pavlovetc, I. M., Collette, R., Kong, X.-T., Rack, P. D., Zhang, S., Masiello, D. J., Camden, J. P., Hartland, G. V., and Kuno, M., "Far-field midinfrared superresolution imaging and spectroscopy of single high aspect ratio gold nanowires," Proc. Natl. Acad. Sci. U.S.A. 117, 2288–2293 (2020).
- [28] Pavlovetc, I. M., Podshivaylov, E. A., Chatterjee, R., Hartland, G. V., Frantsuzov, P. A., and Kuno, M., "Infrared photothermal heterodyne imaging: Contrast mechanism and detection limits," <u>J. Appl. Phys.</u> **127**, 165101 (2020).
- [29] Pavlovetc, I. M., Aleshire, K., Hartland, G. V., and Kuno, M., "Approaches to mid-infrared, super-resolution imaging and spectroscopy," Phys. Chem. Chem. Phys. 22, 4313–4325 (2020).
- [30] Li, C., Zhang, D. L., Slipchenko, M. N., and Cheng, J. X., "Mid-infrared photothermal imaging of active pharmaceutical ingredients at submicrometer spatial resolution," Anal. Chem. 89, 4863–4867 (2017).
- [31] Bai, Y., Zhang, D., Lan, L., Huang, Y., Maize, K., Shakouri, A., and Cheng, J.-X., "Ultrafast chemical imaging by widefield photothermal sensing of infrared absorption," <u>Sci. Adv.</u> 5, eaav7127 (2019).
- [32] Zhang, D., Li, C., Zhang, C., Slipchenko, M. N., Eakins, G., and Cheng, J.-X., "Depth-resolved mid-infrared photothermal imaging of living cells and organisms with submicrometer spatial resolution," <u>Sci. Adv.</u> 2, e1600521 (2016).
- [33] Samolis, P. D. and Sander, M. Y., "Phase-sensitive lock-in detection for high-contrast mid-infrared photothermal imaging with sub-diffraction limited resolution," Opt. Express 41, 2643–2655 (2019).
- [34] Lim, J. M., Park, C., Park, J.-S., Kim, C., Chon, B., and Cho, M., "Cytoplasmic protein imaging with mid-infrared photothermal microscopy: Cellular dynamics of live neurons and oligodendrocytes," <u>J. Phys.</u> Chem. Lett. **10**, 2857–2861 (2019).

- [35] Li, C., Zhang, D. L., Slipchenko, M. N., and Cheng, J. X., "Mie-type scattering and non-beer-lambert absorption behavior of human cells in infrared microspectroscopy," Biophys. J. 88, 3635–3640 (2005).
- [36] Bassan, P., Byrne, H. J., Bonnier, F., Lee, J., Dumas, P., and Gardner, P., "Resonant mie scattering in infrared spectroscopy of biological materials understanding the 'dispersion artefact'," <u>Analyst</u> **134**, 1586–1593 (2009).
- [37] Olson, N. E., Xiao, Y., Lei, Z., and Ault, A. P., "Simultaneous optical photothermal infrared (o-ptir) and raman spectroscopy of submicrometer atmospheric particles," <u>Anal. Chem. 2020, 92, 14, 9932–9939</u> **92**, 9932–9939 (2020).
- [38] Cai, Y., Yang, T., Mitrano, D. M., Heuberger, M., Hufenus, R., and Nowack, B., "Systematic study of microplastic fiber release from 12 different polyester textiles during washing," Environ. Sci. Technol. 54, 4847–4855 (2020).
- [39] Falco, F. D., Pace, E. D., Cocca, M., and Avella, M., "The contribution of washing processes of synthetic clothes to microplastic pollution," Sci. Rep. 9, 6633 (2019).